

Efficient Algorithms for Ptychographic Phase Retrieval

Jianliang Qian, Chao Yang, A. Schirotzek, F. Maia, and S. Marchesini

This paper is dedicated to Prof. Gunther Uhlmann on the occasion of his 60th birthday.

ABSTRACT. Ptychography is an emerging non-crystalline diffractive imaging technique that can potentially reach diffraction limited resolution without the need for high resolution lenses. To achieve high resolution one must solve a phase-retrieval inverse problem using the diffraction patterns of many partially overlapping subimage frames. We examine the mathematical formulation of the ptychographic phase retrieval problem, and analyze some of the existing methods for solving the inverse problem. We also discuss a number of practical techniques that can improve the efficiency and robustness of numerical algorithms for solving the ptychographic phase retrieval problem.

1. Introduction

Ptychography is an emerging non-crystalline diffractive imaging technique by which one can deduce the structure of an object from a number of diffraction patterns; see Figure 1. It can be formulated as an inverse problem in which the phase relationship between different parts of a scattered wave disturbance is deduced from the magnitude of the wave that can be physically measured. Its usefulness lies in its ability to recover structure information without using high resolution lenses or defining properties of the scattering medium. The missing phase information is obtained implicitly from the intensity recorded in the diffraction plane through an iterative computational method [1, 2, 3]. In this paper, we examine the mathematical formulation of the ptychographic phase retrieval problem, and analyze some of the existing algorithms for solving this type of inverse problems.

We consider reconstruction of two-dimensional (2D) objects, although the technique we discuss here can in principle be extended to 3D structure elucidation. In a ptychography experiment, one collects a sequence of diffraction images of dimension $m \times m$. Each image frame $y_{\mathbf{x}}(\mathbf{r}')$ represents the magnitude of the Fourier transform of $a(\mathbf{r})\psi_0(\mathbf{r} + \mathbf{x})$, where $a(\mathbf{r})$ is a localized illumination (window) function or a probe, $\psi_0(\mathbf{r})$ is the unknown object of interest, and \mathbf{x} is a translational vector.

1991 *Mathematics Subject Classification.* Primary 65T50; Secondary 42B99.

Key words and phrases. diffractive imaging, ptychography, phase retrieval, numerical algorithms.

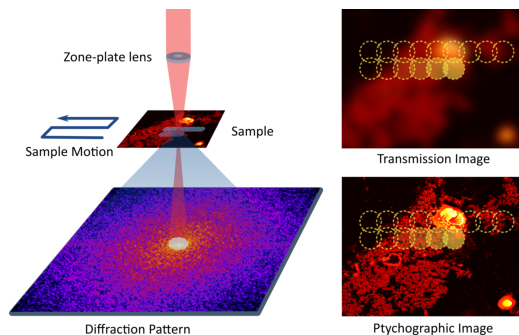


FIGURE 1. A schematic drawing of a ptychography experiment in which a probe scans through a 2D object in an overlapping fashion and produces a sequence of diffraction patterns of the scanned regions.

We can express $y_{\mathbf{x}}$ as

$$(1.1) \quad y_{\mathbf{x}}(\mathbf{r}') = |\mathcal{F}\{a(\mathbf{r})\psi_0(\mathbf{r} + \mathbf{x})\}|,$$

where $\mathcal{F}\{f\}$ denotes the Fourier transform of f with respect to \mathbf{r} .

In order to reconstruct the unknown object, we must retrieve the amplitude and phase of $\psi_0(\mathbf{r})$ from a number of $y_{\mathbf{x}}(\mathbf{r}')$ that are associated with different \mathbf{x} 's. A few methods have been proposed to recover $\psi_0(\mathbf{r})$ from ptychographic measurements $y_{\mathbf{x}}(\mathbf{r}')$ [1, 2, 3, 4, 5]. The connection among these methods is not entirely clear from the existing literature. Furthermore, little detail is provided on convergence properties or computational efficiency of these methods.

In this paper, we analyze some of the existing methods for solving ptychographic phase retrieval problem from a numerical optimization point of view. In particular, we examine the local convergence properties of these methods by analyzing the gradient and Hessian of different objective functions, which we present in section 2. We discuss a number of computational details such as weighting and preconditioning that are important for achieving good performance in these methods in section 3. We also describe the connection between optimization based algorithms and projection algorithms that are frequently used in phase retrieval in section 3.2. A number of computational examples are presented in section 4 to illustrate and compare the convergence behavior of several methods for solving the ptychographic phase retrieval problem.

We point out that the ptychographic minimization problem is not globally convex, which means that iterative methods can be trapped at a local minimizer if a poor starting guess is chosen. We show by a numerical example that one way to escape from a local minimizer is to switch to a different objective function in section 4.

We observed that the convergence of the optimization based iterative algorithms used to perform ptychographic phase retrieval become faster when the amount of overlap between two adjacent image frames increases. We provide a preliminary analysis of how the amount of overlap between adjacent frames affects the convergence of iterative optimization algorithms in section 4.

We use standard linear algebra notation whenever possible to describe various quantities evaluated in the iterative algorithms we present. To simplify notation we use a/b to denote an element-wise division between two vectors a and b . Similarly, we use $a \cdot b$ to denote an element-wise multiplication of a and b . We also use a^2 and $a^{1/2}$ occasionally to denote the element-wise square and square root of a respectively. The conjugate of a complex variable a is denoted by \bar{a} . The real part of a is denoted by $\text{Re}(a)$. The conjugate transpose of a matrix (or a vector) A is denoted by A^* . The $|x|$ symbol is reserved for the magnitude (or absolute value) of x . The Euclidean norm of x is denoted by $\|x\| = \sqrt{x^*x}$. We use $\text{Diag}(x)$ to represent a diagonal matrix with the vector x on its diagonal.

2. Ptychographic reconstruction as an inverse problem

The phase retrieval problem has a long history in both the optics and inverse problem communities. The uniqueness question of phase retrieval has been investigated under various conditions in different contexts [6, 8, 9]. Recently, it has been shown that the problem can be formulated as a low-rank matrix completion problem [10] and solved by convex programming techniques if the standard diffraction experiments can be modified to generate additional information. In this paper, we examine efficient algorithms for solving another special class of phase retrieval problems in which the unknown object ψ_0 is recovered from a number of intensity measurements represented by (1.1). For a finite set of translational vectors \mathbf{x}_i , we will denote each measurement by

$$b_i = |FQ_i\psi_0|, \quad i = 1, 2, \dots, k,$$

where ψ_0 is the sampled unknown object that contains n pixels, b_i is a sampled measurement that contains m pixels, F is the matrix representation of a discrete Fourier transform, and Q_i is an $m \times n$ ‘‘illumination matrix’’ that extracts a frame containing m pixels out of an image containing n pixels. Each row of Q_i contains at most one nonzero element. The nonzero values in Q_i are determined by the illumination function $a(\mathbf{r})$.

Given a set of measurements, b_1, b_2, \dots, b_k , we may attempt to recover ψ_0 by solving either the least squares problem

$$(2.1) \quad \min_{\psi} \rho(\psi) \equiv \min_{\psi} \frac{1}{2} \sum_{i=1}^k \| |z_i| - b_i \|^2, \quad \text{or}$$

$$(2.2) \quad \min_{\psi} \epsilon(\psi) \equiv \min_{\psi} \frac{1}{2} \sum_{i=1}^k \| |z_i|^2 - b_i^2 \|^2,$$

where $z_i \equiv FQ_i\psi$. The advantage of using (2.2) is that it is slightly smoother than (2.1), hence more amenable to analysis. In practice, we found the objective function in (2.1) to be a better choice in terms of computational efficiency in most cases.

To obtain the minimizers of (2.1) or (2.2) using numerical optimization techniques, we often need to evaluate the gradient and possibly the Hessian of these objective functions. Because both (2.1) and (2.2) are real-valued functions of a (potentially) complex vector ψ , one can either take the derivative of (2.1) and (2.2)

with respect to the real and imaginary parts of ψ independently or follow the $\mathbb{C}\mathbb{R}$ -calculus formalism established in [11, 12] by treating ψ and $\bar{\psi}$ as two independent variables. The latter approach is what we use throughout this paper.

2.1. Gradient. If we let $r_i \equiv |z_i|^2 - b_i^2$ and define

$$r \equiv (r_1^T, r_2^T, \dots, r_k^T)^T,$$

we can rewrite (2.2) as $\epsilon(\psi) = r^T r/2$. It is not difficult to show that [13]

$$(2.3) \quad \nabla \epsilon = \sum_{i=1}^k Q_i^* F^* \text{Diag}(z_i) [|z_i|^2 - b_i^2].$$

The gradient of the objective function $\rho(\psi)$ in (2.1) is slightly more complicated. By rewriting $|z_i|$ as $(|z_i|^2)^{1/2}$ and using the chain rule, we obtain

$$(2.4) \quad \nabla \rho(\psi) = \frac{1}{2} \sum_{i=1}^k \left[Q_i^* Q_i \psi - Q_i^* F^* \text{Diag} \left(\frac{z_i}{|z_i|} \right) b_i \right].$$

Note that both (2.3) and (2.4) remain real when ψ is real and when b_i is obtained from a discrete Fourier transform of a real image (so that conjugate symmetry is preserved in $\text{Diag}(z_i/|z_i|) b_i$.)

2.2. Hessian. The Hessians of $\epsilon(\psi)$ and $\rho(\psi)$ provide information on the convexity of these objective functions. Again, because both $\epsilon(\psi)$ and $\rho(\psi)$ are real valued functions of a potentially complex vector ψ , their Hessians are defined as

$$H^f = \begin{pmatrix} H_{\psi\psi}^f & H_{\psi\bar{\psi}}^f \\ H_{\bar{\psi}\psi}^f & H_{\bar{\psi}\bar{\psi}}^f \end{pmatrix},$$

where

$$H_{\psi\psi}^f \equiv \frac{\partial}{\partial \psi} \left(\frac{\partial f}{\partial \psi} \right)^*, \quad H_{\bar{\psi}\psi}^f \equiv \frac{\partial}{\partial \bar{\psi}} \left(\frac{\partial f}{\partial \psi} \right)^*, \quad H_{\psi\bar{\psi}}^f \equiv \frac{\partial}{\partial \psi} \left(\frac{\partial f}{\partial \bar{\psi}} \right)^*, \quad H_{\bar{\psi}\bar{\psi}}^f \equiv \frac{\partial}{\partial \bar{\psi}} \left(\frac{\partial f}{\partial \bar{\psi}} \right)^*,$$

and f is either ϵ or ρ .

It is not difficult to show that [13]

$$H^\epsilon = \begin{pmatrix} \sum_i Q_i^* F^* \text{Diag}(2|z_i|^2 - b_i^2) F Q_i & \sum_i Q_i^* F^* \text{Diag}(z_i)^2 \overline{F Q_i} \\ \sum_i Q_i^T F^T \text{Diag}(\bar{z}_i)^2 F Q_i & \sum_i Q_i^T F^T \text{Diag}(2|z_i|^2 - b_i^2) \overline{F Q_i} \end{pmatrix}.$$

If we let $t_{ji} \equiv |t_{ji}| e^{i\mu_{ji}}$, $\zeta_{ji} \equiv |\zeta_{ji}| e^{i\theta_{ji}}$ and β_{ji} be the j th component of $t_i = F Q_i \phi$, $z_i = F Q_i \psi$ and b_i respectively, then the curvature $\tau_\epsilon(\psi, \phi)$ at ψ along any direction ϕ can be shown to be

$$(2.5) \quad \begin{aligned} \tau_\epsilon(\psi, \phi) &= (\phi^* \quad \phi^T) \begin{pmatrix} H_{\psi\psi}^\epsilon & H_{\psi\bar{\psi}}^\epsilon \\ H_{\bar{\psi}\psi}^\epsilon & H_{\bar{\psi}\bar{\psi}}^\epsilon \end{pmatrix} \begin{pmatrix} \phi \\ \bar{\phi} \end{pmatrix} \\ &= 2 \sum_{i=1}^k \sum_{j=1}^n |t_{ji}|^2 (|z_{ji}|^2 - \beta_{ji}^2) + 2 |t_{ji}|^2 |z_{ji}|^2 \cos^2(\mu_{ji} - \theta_{ji}). \end{aligned}$$

At the minimizer of $\epsilon(\psi)$, $|z_i| = b_i$. So the first term of (2.5) is zero. Because the second term of (2.5) is nonnegative, $\tau \geq 0$, i.e., ϵ is locally convex at the solution. Moreover, the convexity of ϵ is preserved in the area where $|z_{ji}| \geq \beta_{ji}$.

A similar observation can be made from the curvature of ρ . It is not difficult to show that

$$H^\rho = \begin{pmatrix} \sum_{i=1}^k W_i^* \left[\frac{1}{2}I - \frac{1}{4}\text{Diag} \left(\frac{b_i}{|z_i|} \right) \right] W_i & \frac{1}{4} \sum_{i=1}^k W_i^* \text{Diag} \left(\frac{b_i \cdot z_i^2}{|z_i|^3} \right) \bar{W}_i \\ \frac{1}{4} \sum_{i=1}^k W_i^T \text{Diag} \left(\frac{b_i \cdot z_i^2}{|z_i|^3} \right) W_i & \sum_{i=1}^k W_i^T \bar{Q}_i \left[\frac{1}{2}I - \frac{1}{4}\text{Diag} \left(\frac{b_i}{|z_i|} \right) \right] \bar{W}_i \end{pmatrix},$$

where $W_i = FQ_i$. It follows that

$$(2.6) \quad \tau_\rho(\psi, \phi) = \sum_{i=1}^k \sum_{j=1}^n |t_{ji}|^2 \left(1 - \frac{\beta_{ji}}{|\zeta_{ji}|} \sin^2(\mu_{ji} - \theta_{ji}) \right).$$

Thus, $\tau_\rho \geq 0$ when $|\zeta_{ji}| \geq \beta_{ji}$ for all $j = 1, 2, \dots, n$ and $i = 1, 2, \dots, k$. Even if $|\zeta_{ji}|$ is slightly less than β_{ji} for some j and i , τ_ρ may remain positive when the corresponding $\sin^2(\mu_{ji} - \theta_{ji})$ is sufficiently small and other terms in the summation in (2.6) are sufficiently large and positive.

A classical problem encountered in optics is associated with $k = 1$. When only one diffraction image is recorded, experience shows that local minima are common. Regions of negative curvature separate local minima from the global solution [16].

3. Iterative algorithms based on nonlinear optimization

Because the gradient and Hessian of (2.1) and (2.2) are relatively easy to evaluate, we may use standard minimization algorithms such as the steepest descent method, the Newton's method and the nonlinear conjugate gradient method to find the solution to the ptychographic reconstruction problem.

3.1. Unconstrained minimization. When the objective function (2.1) or (2.2) is minimized directly, we construct a sequence of approximations to ψ_0 by

$$(3.1) \quad \psi^{(\ell+1)} = \psi^{(\ell)} + \beta p^{(\ell)},$$

where $p^{(\ell)}$ is a *search direction* along which the objective function (2.1) or (2.2) decreases, and $\beta > 0$ is an appropriate step length chosen through a line search procedure that ensures global convergence [17]. Global convergence can also be achieved by introducing an additional inequality constraint that limits the size of the update within a “trust region” [18].

To accelerate convergence, we may also introduce an appropriate weighting matrix into least squares objective functions (2.1) and (2.2) by expressing them as

$$\rho(\psi) = \frac{1}{2} \sum_{i=1}^k \langle |z_i| - b_i, |z_i| - b_i \rangle_B,$$

and

$$\epsilon(\psi) = \frac{1}{2} \sum_{i=1}^k \langle |z_i|^2 - b_i^2, |z_i|^2 - b_i^2 \rangle_B$$

respectively, where $\langle x, y \rangle_B = x^* B y$ with B being a symmetric positive definite matrix. As we will show in section 4, the choice of $B = \text{Diag}(b_i)^{-1}$ is particularly useful for accelerating the convergence of all iterative methods we have looked at. To maintain numerical stability and reduce noise amplification, it is often necessary to add a small constant to the diagonal of B to prevent it from becoming singular or ill-conditioned. In the presence of noise, the choice of B can be made according

to a stochastic characterization of the noise. This leads to a maximum likelihood formulation of the phase retrieval problem [15].

Another useful technique for accelerating iterative methods for solving unconstrained minimization problems is preconditioning. Instead of minimizing $\rho(\psi)$ or $\epsilon(\psi)$, we make a change of variable and minimize $\hat{\rho}(\phi)$ and $\hat{\epsilon}(\phi)$, where $\phi = K\psi$, and K is a preconditioner that is usually required to be Hermitian and positive definite. The purpose of introducing the preconditioner K is to reduce the condition number of the Hessian of the objective function. A highly ill-conditioned Hessian often leads to slow convergence of an iterative method. A well-known example is the zig-zag behavior of the steepest descent algorithm when it is applied to the Rosenbrock function.

It follows from the chain rule and (2.4) that the gradient of $\hat{\rho}(\psi)$ is simply

$$\nabla \hat{\rho}(\psi) = \frac{1}{2} K^{-1} \sum_{i=1}^k [Q_i^* Q_i \psi - Q_i^* F^* \text{Diag} \left(\frac{z_i}{|z_i|} \right) b_i],$$

where $z_i = FQ_i\psi$.

If we take the preconditioner to be the constant term on the diagonal blocks of $H_{\psi\psi}^{\rho}$, i.e.,

$$(3.2) \quad K = \sum_{i=1}^k Q_i^* Q_i,$$

which is a diagonal matrix, the gradient of $\hat{\rho}$ simply becomes

$$\nabla \hat{\rho}(\psi) = \frac{1}{2} \left[\psi - \left(\sum_{i=1}^k Q_i^* Q_i \right)^{-1} \left(\sum_{i=1}^k Q_i^* F^* \text{Diag} \left(\frac{z_i}{|z_i|} \right) b_i \right) \right],$$

and the corresponding preconditioned steepest descent algorithm with a constant step length of 2 yields the following updating formula:

$$\psi^{(\ell+1)} = \left(\sum_{i=1}^k Q_i^* Q_i \right)^{-1} \left(\sum_{i=1}^k Q_i^* F^* \text{Diag} \left(\frac{z_i^{(\ell)}}{|z_i^{(\ell)}|} \right) b_i \right),$$

where $z_i^{(\ell)} = FQ_i\psi^{(\ell)}$. This updating formula is identical to that used in the *error reduction* algorithm or *alternate projection* algorithm [16], which is guaranteed to converge to at least a local minimizer as shown in section 3.2.

3.2. Fixed-point iteration and projection algorithms. An alternative approach to finding a minimizer of (2.1) is to set its gradient to zero and seek ψ that satisfies the first order necessary condition of the minimization problem. If $\sum_{i=1}^k Q_i^* Q_i$ is nonsingular, by setting $\nabla \rho(\psi) = \frac{1}{2} \sum_{i=1}^k [Q_i^* Q_i \psi - Q_i^* F^* \text{Diag} \left(\frac{z_i}{|z_i|} \right) b_i]$ to 0, we obtain

$$(3.3) \quad \psi = f(\psi)$$

where

$$(3.4) \quad f(\psi) = \left(\sum_{i=1}^k Q_i^* Q_i \right)^{-1} \left[\sum_{i=1}^k Q_i^* F^* \text{Diag} \left(\frac{z_i}{|z_i|} \right) b_i \right].$$

Recall that $z_i \equiv FQ_i\psi$. Clearly, ψ is a fixed point of the function f .

A simple iterative technique one may use to find the solution to (3.4) is the fixed point iteration that has the form

$$\psi^{(\ell+1)} = f(\psi^{(\ell)}).$$

Replacing f with the right hand side of (3.4) yields

$$(3.5) \quad \psi^{(\ell+1)} = \left(\sum_{i=1}^k Q_i^* Q_i \right)^{-1} \left[\sum_{i=1}^k Q_i^* F^* \text{Diag} \left(\frac{z_i^{(\ell)}}{|z_i^{(\ell)}} \right) b_i \right],$$

where $z_i^{(\ell)} \equiv F Q_i \psi^{(\ell)}$. This is the same sequence of iterates produced in what is known as the *error reduction* algorithm in standard phase retrieval literature [16]. This method is also known as the *alternate projection* algorithm for reasons to be discussed below.

It is easy to verify that the updating formula in (3.5) is identical to that produced by a preconditioned steepest descent algorithm in which the preconditioner K is chosen to be $K = \sum_{i=1}^k Q_i^* Q_i$, and a constant step length of 2 is taken at each iteration, i.e.,

$$\psi^{(\ell+1)} = \psi^{(\ell)} - 2 \nabla \rho(\psi^{(\ell)}).$$

The sequence of iterates $\{\psi^{(\ell)}\}$ produced by (3.5) is guaranteed to converge to the fixed point of $f(\psi)$ from any starting point $\{\psi^{(0)}\}$, if the spectral radius (i.e., the largest eigenvalue) of the Jacobian of f (with respect to ψ) is strictly less than 1. Because the function f in (3.3) can be viewed as a function of ψ and $\bar{\psi}$, we should examine the Jacobian matrix of the system

$$(3.6) \quad \psi = \left(\sum_{i=1}^k Q_i^* Q_i \right)^{-1} \left[\sum_{i=1}^k Q_i^* F^* \text{Diag} \left(\frac{z_i}{|z_i|} \right) b_i \right],$$

$$(3.7) \quad \bar{\psi} = \left(\sum_{i=1}^k Q_i^T \bar{Q}_i \right)^{-1} \left[\sum_{i=1}^k Q_i^T F^T \text{Diag} \left(\frac{\bar{z}_i}{|\bar{z}_i|} \right) b_i \right],$$

where (3.7) is simply the conjugate of (3.6). It is not difficult to show that this Jacobian matrix has the form

$$(3.8) \quad J = \begin{pmatrix} K^{-1} & 0 \\ 0 & \bar{K}^{-1} \end{pmatrix} \begin{pmatrix} K - 2H_{\psi\psi}^\rho & -2H_{\psi\bar{\psi}}^\rho \\ -2H_{\bar{\psi}\psi}^\rho & \bar{K} - 2H_{\bar{\psi}\bar{\psi}}^\rho \end{pmatrix},$$

where $H_{\psi\psi}^\rho$, $H_{\psi\bar{\psi}}^\rho$, $H_{\bar{\psi}\psi}^\rho$ and $H_{\bar{\psi}\bar{\psi}}^\rho$ are as defined in the formula for H^ρ .

If (λ, ϕ) is an eigenpair of J , we can easily show that

$$2 \begin{pmatrix} H_{\psi\psi}^\rho & H_{\psi\bar{\psi}}^\rho \\ H_{\bar{\psi}\psi}^\rho & H_{\bar{\psi}\bar{\psi}}^\rho \end{pmatrix} \begin{pmatrix} \phi \\ \bar{\phi} \end{pmatrix} = (1 - \lambda) \begin{pmatrix} K & 0 \\ 0 & \bar{K} \end{pmatrix} \begin{pmatrix} \phi \\ \bar{\phi} \end{pmatrix}.$$

If we again let $t_{ji} \equiv |t_{ji}| e^{i\mu_{ji}}$, $\zeta_{ji} \equiv |\zeta_{ji}| e^{i\theta_{ji}}$ and β_{ji} be the j th component of the vectors $t_i = F Q_i \phi$, $z_i = F Q_i \psi$ and b_i respectively, we can easily show that

$$(3.9) \quad \lambda = \frac{\sum_{i=1}^k \sum_{j=1}^n \sin^2(\mu_{ji} - \theta_{ji}) |t_{ji}|^2 \beta_{ji} / |\zeta_{ji}|}{\sum_{i=1}^k \sum_{j=1}^n |t_{ji}|^2}.$$

Clearly, when $\beta_{ji} \leq |\zeta_{ji}|$ for all $j = 1, 2, \dots, m$ and $i = 1, 2, \dots, n$, $|\lambda| \leq 1$, and the fixed point iteration is guaranteed to converge to at least a local minimizer of ρ .

The fixed point of f may also be obtained by applying Newton's method or a quasi-Newton algorithm to seek the root of $r(\psi) = 0$, where $r(\psi) = \psi - f(\psi)$.

This approach is equivalent to applying Newton's method or a quasi-Newton algorithm (with appropriate line search and trust region strategies) to minimize $\rho(\psi)$.

If we multiply (3.6) from the left by Q_i for $i = 1, 2, \dots, k$, and let $y^{(\ell)} = Q\psi^{(\ell)}$, where $Q = (Q_1^* \ Q_2^* \ \dots \ Q_k^*)^*$, we obtain

$$(3.10) \quad y^{(\ell+1)} = P_Q P_F(y^{(\ell)}),$$

where $P_Q = Q(Q^*Q)^{-1}Q^*$, and

$$P_F(y) = \hat{F}^* \frac{y}{|y|} \cdot b,$$

where $\hat{F} = \text{Diag}(F, F, \dots, F)$ and $b = (b_1^T \ b_2^T \ \dots \ b_k^T)^T$.

Because a fixed point y of $P_Q P_F$ is in the range of Q , which is typically full rank when $mk > n$, we may recover the corresponding fixed point of f from y via the least squares solution $\psi^{(\ell)} = (Q^*Q)^{-1}Q^*y^{(\ell)}$.

This nonlinear map is the composition of a (linear) orthogonal projector P_Q and a (nonlinear) Fourier magnitude projector P_F . A fixed point iteration based on (3.10) is also called *alternating projection* (AP) algorithm in the phase retrieval literature because the approximation to the solution of (3.10) is obtained by applying P_Q and P_F in an alternating fashion.

It is easy to verify that P_F is indeed a projection operator in the sense that

$$(3.11) \quad \|P_F(y) - y\| \leq \|w - y\| \quad \text{for all } w \in \{w | w = P_F(w)\}.$$

This property of P_F , together with the fact that P_Q is an orthogonal projection operator, i.e. $\|P_Q y - y\| \leq \|w - y\|$ for all $w \in \text{Range}(Q)$, allows us to show that the residual error $\|P_F(y^{(\ell)}) - y^{(\ell)}\|$ decreases monotonically in the AP algorithm. The proof of this observation was provided by Fienup in [19].

The simple alternating projection algorithm has been extended to the hybrid input-output (HIO) algorithm [19], the relaxed averaged alternating reflection (RAAR) algorithm [20], and many other variants [21, 16] in the phase retrieval literature. Just to give a few examples, in the HIO and RAAR algorithms, the approximation to the solutions of (3.7) and (3.10) are updated by

$$\begin{aligned} y^{(\ell+1)} &= [P_Q P_F + (I - P_Q)(I - \beta P_F)] y^{(\ell)}, \quad \text{and} \\ y^{(\ell+1)} &= [2\beta P_Q P_F + (1 - 2\beta)P_F + \beta(P_Q - I)] y^{(\ell)}, \end{aligned}$$

respectively, where β is a constant often chosen to be between 0 and 1, and the object itself can be recovered from $y^{(\ell)}$ through $\psi^{(\ell+1)} = (Q^*Q)^{-1}Q^*y^{(\ell)}$.

Although these algorithms tend to accelerate the convergence of $y^{(\ell)}$, their convergence behavior is less predictable and not well understood.

4. Numerical examples

In this section, we demonstrate and compare the convergence of iterative algorithms for ptychographic reconstruction using two test images. The first test image is a 256×256 real-valued cameraman image shown in Figure 2. The image is often used in the image processing community to test image reconstruction and restoration algorithms. The second test image is a complex valued image. It also contains 256×256 pixels that correspond to the complex transmission coefficients

of a collection of gold balls embedded in some medium. The amplitude and phase angles of these pixels are shown in Figure 3.

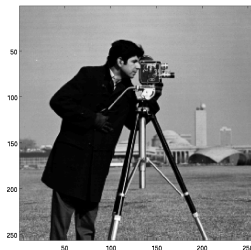


FIGURE 2. The cameraman test image.

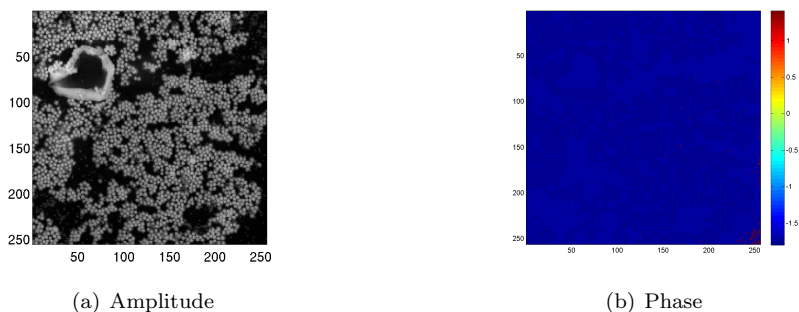


FIGURE 3. The amplitude and phase of the transmission coefficient of a collection of gold balls.

All numerical examples presented in this paper are performed in MATLAB.

4.1. Numerical comparison of iterative methods. In this section, we show the convergence behavior of a few iterative algorithms for solving the ptychographic reconstruction by numerical experiments. In the cameraman image reconstruction experiment, we choose the illuminating probe $a(\mathbf{r})$ to be a 64×64 binary probe shown in Figure 4(a). The pixels within the 32×32 square at the center of the probe assume the value of 1. All other pixels take the value of 0. The zero padding of the inner 32×32 square ensures that the diffraction pattern of a 64×64 frame associated with this probe is oversampled in the reciprocal space. In the gold ball image reconstruction experiment, the illuminating probe is chosen to be the amplitude of the Fourier transform of an annular ring with inner radius of $r_1 \approx 5.4$ and outer radius of $r_2 \approx 19.4$. This probe mimics the true illumination used in a physical experiment.

In the cameraman experiment, the probe is translated by 8 pixels at a time in either horizontal or vertical direction. To prepare a stack of k diffraction images b_i , $i = 1, 2, \dots, k$, we start from the upper left corner of the true image, extract a



(a) The binary probe used in the reconstruction of the cameraman image.

(b) The probe used in the reconstruction of the gold ball image.

FIGURE 4. The illuminating probes $a(\mathbf{r})$ used in ptychographic reconstructions of the cameraman and gold ball images.

64×64 frame, and multiply it with the probe, and then apply a 2D FFT to the product. The magnitude of transform is recorded and saved before we move either horizontally or vertically to obtain the next frame. If the lower right corner of the frame goes outside of the image (which does not happen in this particular case), we simply “wrap the probe around” the image as if the image is periodically extended. As a result, the total number of diffraction frames we use for each reconstruction is $k = (256/8) \cdot (256/8) = 1024$.

As we will show in section 4.3, the size of translation, which determines the amount of overlap between adjacent frames, has a noticeable effect on the convergence of the iterative reconstruction algorithms.

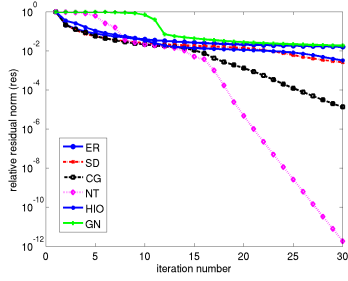
Figure 5 shows the convergence history of several iterative algorithms discussed in section 3 when they are applied to the diffraction frames extracted from the cameraman image. We plot both the relative residual norm defined by

$$(4.1) \quad res = \frac{\sqrt{\sum_{i=1}^k \| |z_i|^{(\ell)} - b_i \|^2}}{\sqrt{\sum_{i=1}^k \| b_i \|^2}},$$

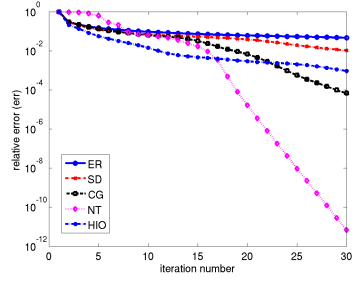
where $|z_i|^{(\ell)} = |FQ_i\psi^{(\ell)}|$ and ℓ is the iteration number, and the relative error of the reconstructed image defined by $err = \|\psi^{(\ell)} - \psi_0\|/\|\psi_0\|$. In these runs, an exact line search is used in both the steepest descent (SD) method and the nonlinear conjugate gradient (CG) method. The Steihaug’s trust region technique [23] is used in the Newton’s method (NT). We set the starting guess of the solution ψ_0 to

$$\psi^{(0)} = \left(\sum_{i=1}^k Q_i^* Q_i \right)^{-1} \sum_{i=1}^k Q_i^* b_i.$$

It is clear from Figure 5 that NT converges much faster than the other algorithms. Its performance is followed by the CG algorithm which is much faster than the error reduction (ER), SD, Gauss-Newton (GN) and the hybrid input-output (HIO) algorithms. Similar convergence behavior is observed when other random starting guesses are used, although occasionally, a random starting guess can lead to stagnation or convergence to a local minimizer. We will discuss this issue in section 4.2.



(a) Change of the relative residual norm (res) for the reconstruction of the cameraman image.



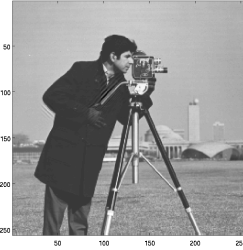
(b) Change of the relative error (err) for the reconstruction of the cameraman image.

FIGURE 5. A comparison of the convergence behavior of different iterative ptychographic reconstruction algorithms for the cameraman image.

We set the maximum number of iterations allowed in all runs to 30. This is somewhat excessive for both NT and CG algorithms. Typically, when the relative error of the reconstructed image falls below 10^{-3} , it is nearly impossible to visually distinguish the reconstruction from the true image. When the relative error is larger, the reconstructed cameraman images may contain visible artifacts such as those shown in Figures 6(a) and 6(b) which are produced at the end of the 30th ER and SD iterations respectively.



(a) ER reconstruction



(b) SD reconstruction

FIGURE 6. The reconstructed cameraman images by ER and SD algorithms contain visible ringing artifacts.

For the reconstruction of the gold ball image, we choose the starting guess to be

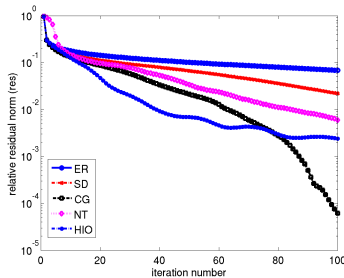
$$\psi^{(0)} = \left(\sum_{i=1}^k Q_i^* Q_i \right)^{-1} \sum_{i=1}^k Q_i^* \text{Diag}(b_i) \text{Diag}(|u_i|)^{-1} u_i,$$

where u_i is a complex random vector, and the real and imaginary part of each component has a uniform distribution within $[-1, 1]$.

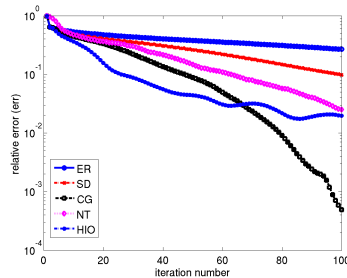
In this experiment, the probe is translated by a larger amount (16 pixels) in either horizontal or vertical direction. Figure 7 shows the convergence history of

ER, SD, CG, HIO, and NT. From Figure 7(a), it appears that CG is the best among all the methods we tried. The HIO algorithm performs well in the first 60 iterations, but then stagnates. As we can see from Figure 7 that neither the residual norm nor the relative error associated with HIO changes monotonically. This is not completely surprising because HIO does not try to minimize either objective functions. For this example, the performance of NT lags behind CG by a large margin although both algorithms exhibit monotonic convergence with a more predictable error reduction. We should mention that to measure the relative error associated with a reconstructed gold ball image $\psi^{(\ell)}$, we need to multiply it by a constant phase factor γ first, i.e., the relative error is defined as

$$err = \frac{\|\gamma\psi^{(\ell)} - \psi_0\|}{\|\psi_0\|}.$$



(a) Change of the relative residual norm (res) for the reconstruction of the gold ball image.



(b) Change of the relative error (err) for the reconstruction of the gold ball image.

FIGURE 7. A comparison of the convergence behavior of different iterative ptychographic reconstruction algorithms for the gold ball image.

4.2. Local minimizer and the choice of the objective function. As we indicated in section 2.2, based on the analytic Hessian and curvature expression, neither $\epsilon(\psi)$ nor $\rho(\psi)$ is globally convex. This observation suggests that all iterative optimization algorithm discussed above may converge to a local minimizer. Although we found that in practice, local minimizers are not easy to find, they do exist as the following example shows.

In order to find a local minimizer, we construct many random starting guesses using the MATLAB `rand` function. To save time, we choose to reconstruct a 64×64 subimage of the cameraman image shown in Figure 2. This subimage is shown in Figure 10(a). A 16×16 binary probe that has a value 1 in the 8×8 center of the probe and 0 elsewhere is used. The diffraction stack consisting of 64 diffraction images is obtained by translating the probe 4 pixels a time in either the horizontal or the vertical direction.

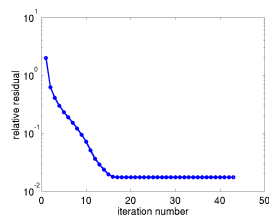
Figure 8 shows that one of the random starting guesses leads to the convergence of the CG algorithm to a local minimizer. In particular, the relative residual (4.1) which is proportional to the objective function ρ stagnates around 0.9 after the first

15 iterations (Figure 8(a)), whereas the relative gradient $\|\nabla\rho(\psi^{(\ell)})\|/\|\psi_0\|$ decreases to 10^{-8} after 40 iterations.

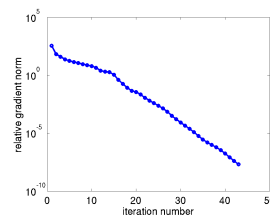
Figure 10(b) shows how the reconstructed image compares with the true image for this particular starting guess used. In this case, the local minimizer appears to contain visible artifacts in a small region near top of the tripod. The amplitude of this localized error is also revealed in the relative error plot shown in Figure 9(a). The phase error associated with a particular frame of the reconstruction obtained from

$$\frac{\overline{Q_i\psi}}{|Q_i\psi|} \cdot \frac{Q_i\psi_0}{|Q_i\psi_0|},$$

for some particular Q_i is shown in Figure 9(b).

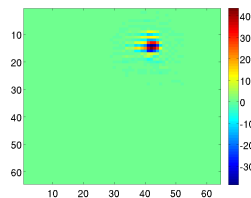


(a) Change of the relative residual norm (res).

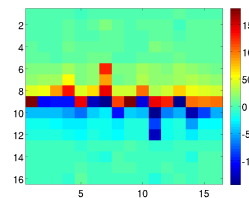


(b) Change of the relative gradient.

FIGURE 8. The convergence of CG to a local minimizer.



(a) Amplitude error in the reconstruct image



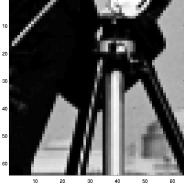
(b) Phase error in degrees associated with a particular frame

FIGURE 9. The error associated with a local minimizer.

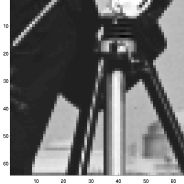
We should also note that for this particular starting guess, all methods we tried converged to the same local minimizer. This is not all that surprising. It simply shows (empirically) that a local minimizer of (2.1) exists, and our starting guess is sufficiently close to it.

However, what is interesting is that if we choose to minimize (2.2) by using any one of the iterative methods discussed above from the same starting guess, we are able to obtain the correct solution. For example, Figure 11(a) shows that when the NT applied to the weighted (scaled) objective function

$$(4.2) \quad \tilde{\epsilon}(\psi) = \frac{1}{2} \sum_{i=1}^k (|z_i|^2 - b_i^2)^T \text{Diag}(b_i)^{-1} (|z_i|^2 - b_i^2),$$



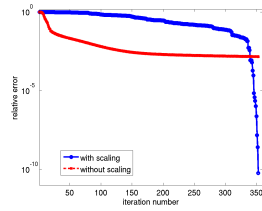
(a) True image.



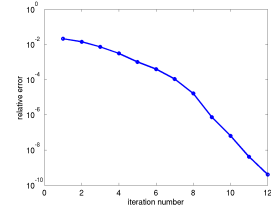
(b) The reconstructed image (a local minimizer).

FIGURE 10. The artifacts produced by a local minimizer of ρ .

where $|z_i| = |FQ_i\psi|$ and $b_i = |FQ_i\psi_0|$, an accurate reconstruction can be obtained in roughly 350 iterations. Admittedly, the convergence rate is much slower in this case when compared to the convergence of NT applied to (2.1) from a different starting point. The convergence is even slower if no weighting (or scaling) is used, i.e. when (2.2) is used as the objective function. However, the fact that convergence can be reached for (4.2) but not (2.1) from the same starting point is quite interesting. Furthermore, Figure 11(b) shows that if we take the local minimizer returned from an iterative minimization of (2.1) as the starting guess for minimizing (4.2), convergence can be reached in 12 iterations. This experiment suggests that it may be useful to have a hybrid optimization scheme in which (2.1) is minimized first. If a local minimizer of (2.1) is identified, one can then try to minimize (4.2) starting from the local minimizer of (2.1). A local minimizer can be recognized by examining the norm of gradient, which should be very small, and the objective function (2.1) or (2.2) itself, which is not close to zero at a local minimizer.



(a) The convergence of the NT algorithm when it is applied to (2.2) (red) and (4.2). The starting guess chosen in these runs is the same one used in the minimization of (2.1).



(b) The convergence of the NT algorithm when the starting guess is chosen to be the local minimizer shown in Figure 10(b)

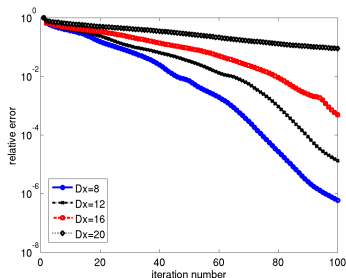
FIGURE 11. The convergence of the NT algorithm when applied to (2.2) (red) and (4.2) (blue).

4.3. The effect of overlapping on the convergence of iterative algorithm. When there is no overlap between two adjacent frames, the ptychographic phase retrieval problem reduces to that of classical phase retrieval for a number

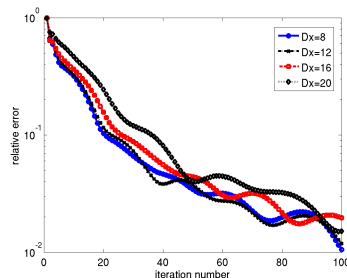
of isolated diffraction images. For this type of problems, optimization based algorithms often converge to a local minimizer. On the other hand, when all frames completely overlap, the phase retrieval problem is equally difficult to solve because overlapping does not provide any new information and phase retrieval is essentially performed on a single diffraction image.

Apart from these two extreme cases, having significant overlap among adjacent frames as we move the probe generally helps improve the convergence of optimization algorithms. The following example show that the amount of overlap has a noticeable effect on the convergence of optimization based iterative algorithms (e.g., CG, NT, SD etc.) A similar observation is also reported in [24].

In this example, we try to reconstruct the gold ball image from four different diffraction stacks. Each stack contains a set of 64×64 diffraction frames. These frames are generated by translating the probe shown in Figure 4(b) by different amount (Δx) in horizontal and vertical directions. The larger the translation, the smaller the overlap is between two adjacent images. Figure 12(a) shows that CG converges very slowly when the diffraction stack contains diffraction frames obtained by translating the probe 20 pixels at a time (the black curve). Faster convergence is observed when the amount of translation is decreased to $\Delta x = 16, 12, 8$. It is interesting to see from Figure 12(b) that the amount of overlap does not affect the convergence of the HIO algorithm.



(a) The effect of overlapping on the convergence of CG for the gold ball image reconstruction.



(b) The effect of overlapping on the convergence of HIO for the gold ball image reconstruction.

FIGURE 12. The effect of overlapping on the convergence of CG and HIO algorithms.

To explain the effect of overlapping on the convergence of optimization based iterative algorithms such as the nonlinear CG, we examine the structure of the Hessian of the objective function ρ in (2.1). It is not difficult to show [13] that H^ρ can be written as

$$(4.3) \quad H^\rho = \begin{pmatrix} (\hat{F}Q)^* & \\ & (\hat{F}Q)^T \end{pmatrix} \begin{pmatrix} B_{11} & B_{12} \\ B_{21} & B_{22} \end{pmatrix} \begin{pmatrix} \hat{F}Q \\ \overline{\hat{F}Q} \end{pmatrix},$$

where $B_{11} = \overline{B_{22}}$ and $B_{12} = B_{21}^*$ are all diagonal, \hat{F} is a block diagonal matrix of discrete Fourier transforms, i.e. $\hat{F} = \text{Diag}(F, F, \dots, F)$, and $Q = (Q_1^* Q_2^* \dots Q_k^*)^*$. The diagonal elements of B_{11} and B_{12} are simply $1 - \beta_{ji}/(2\zeta_{ji})$ and $\beta_{ji}\zeta_{ji}^2/(2|\zeta_{ji}|^3)$ respectively for $i = 1, 2, \dots, k$ and $j = 1, 2, \dots, m$.

We will show that H^ρ is diagonal-dominant when there is a sufficient amount of overlap between adjacent diffraction frames. To simplify our discussion, let us assume for the moment that b_i is a 1D diffraction pattern obtained from a binary probe that illuminates three pixels at a time, and the probe is translated one pixel at a time so that the adjacent image frames overlap by two pixels. In this case, the $\hat{F}Q$ term in (4.3) has the form

$$\begin{pmatrix} f_1 & f_2 & f_3 & \dots & 0 \\ 0 & f_2 & f_3 & \ddots & \vdots \\ 0 & 0 & f_3 & \ddots & f_k \\ f_1 & 0 & 0 & \ddots & f_k \\ f_1 & f_2 & 0 & \dots & f_k \end{pmatrix},$$

where f_i is the i th column of F .

As a result, a typical diagonal term of H^ρ has the form

$$(4.4) \quad H_{i,i}^\rho = f_i^* D_{i-2} f_i + f_i^* D_{i-1} f_i + f_i^* D_i f_i = \text{trace}(D_{i-2} + D_{i-1} + D_i),$$

where D_i is a diagonal matrix that contains elements $1 - \beta_{ji}/(2\zeta_{ji})$ for $j = 1, 2, 3$.

When ψ is near the solution, z_i is close to b_i . Hence, D_i is likely to contain positive entries only. Therefore, the diagonal elements of H^ρ are likely to be much larger compared to the nonzero off-diagonal elements which contain terms in the form of either $f_j^* D_i f_\ell$ and its conjugate, where $j \neq \ell$, or $f_j^T E_i f_j$ and its conjugate, where E_i is a diagonal matrix (and part of B_{12}) that contains elements $\beta_{ji} \zeta_{ji}^2 / (2|\zeta_{ji}|^3)$ for $j = 1, 2, 3$. Due to the phase difference between f_j and f_ℓ , D_i 's do not add up "coherently" on the off-diagonal of H^ρ as they do on the diagonal. Neither do nonzero entries in E_i 's add up coherently on the off-diagonal blocks of H^ρ . Hence, the matrix H^ρ becomes diagonal-dominant when there is a large amount of overlap between two adjacent frames. In fact, the diagonal of H^ρ may become so dominant that the spectral property of H^ρ is determined largely by the diagonal part of the matrix, which is typically well conditioned due to the averaging of D_i in (4.4). This observation provides an intuitive explanation on why increasing the amount of overlap between adjacent frames tends to improve the convergence rate of CG and other optimization based iterative ptychographical phase retrieval algorithms. Although this is not a precise analysis of the spectral property of H^ρ , the analysis does match with observations made in our numerical experiments. Moreover, this type of analysis can be extended to the 2D case in which F is represented as a tensor product of two 1D discrete Fourier transforms.

5. Conclusion

We formulated the ptychographic phase retrieval problem as a nonlinear optimization problem and discussed how standard iterative optimization algorithms can be applied to solve this problem. We showed that the optimization problems we solve are not globally convex. Hence standard optimization algorithms can produce local minimizers. However, the Hessians of the objective functions we minimize do have special structures that may be exploited.

We compared the performance of several optimization algorithms and found that both Newton's method with Steihaug's trust region technique and the nonlinear conjugate gradient algorithm are efficient for solving this type of problems.

An even more efficient algorithm based on an augmented Lagrangian formulation the problem and the use alternating direction method has recently developed by authors in [25].

We demonstrated by a numerical example that the convergence rate of an optimization algorithm depends on the amount of overlapping between two adjacent diffraction frames. We provided a preliminary analysis on why this occurs. More research is needed to provide a more rigorous study on this phenomenon.

In practice, the diffraction measurements often contain some noise. As a result, regularization techniques must be used in the iterative reconstruction algorithms to limit the amplification of noise. For most of the iterative algorithms described in this paper, regularization amounts to terminating the iterations early [26]. Other regularization techniques include reformulating the problem as a maximum likelihood estimation problem [15] and imposing additional constraints to the optimization problem [7], which can be solved by an augmented projection method [7]. We will describe and compare these technique in a future publication.

Acknowledgment

This work was supported by the Laboratory Directed Research and Development Program of Lawrence Berkeley National Laboratory under the U.S. Department of Energy contract number DE-AC02-05CH11231 (C. Y., A. S., S. M.), the National Science Foundation Grant (J. Q.) and by the Director, Office of Science, Advanced Scientific Computing Research, of the U.S. Department of Energy under Contract No. DE-AC02-05CH11231 (F.M.). The computational results presented were obtained at the National Energy Research Scientific Computing Center (NERSC), which is supported by the Director, Office of Advanced Scientific Computing Research of the U.S. Department of Energy under contract number DE-AC02-05CH11232.

References

- [1] J. M. Rodenburg and R. H. T. Bates. The theory of super-resolution electron microscopy via Wigner-distribution deconvolution. *Phil. Trans. R. Soc. Lond. A*, 339:521–553, 1992.
- [2] H. M. L. Faulkner and J. M. Rodenburg. Movable aperture lensless transmission microscopy: a novel phase retrieval algorithm. *Phy. Rev. Lett.*, 93:023903, 2004.
- [3] J. M. Rodenburg and H. M. L. Faulkner. A phase retrieval algorithm for shifting illumination. *Appl. Phys. Lett.*, 85:4795–4797, 2004.
- [4] M. Guizar-Sicairos and J. R. Fineup. Phase retrieval with transverse translation diversity: a nonlinear optimization approach. *Opt. Express*, 16:7264–7278, 2008.
- [5] P. Thibault, M. Dierolf, O. Bunk, A. Menzel, and F. Pfeiffer. Probe retrieval in ptychographic coherent diffractive imaging. *Ultramicroscopy*, 109:338–343, 2009.
- [6] M. Hayes. The reconstruction of a multidimensional sequence from the phase or magnitude of its Fourier transform. *IEEE Trans. Acoust., Speech, Signal Proc.*, 30:140–154, 1982.
- [7] S. Marchesini, A. Schirotzek, C. Yang, H. Wu and F. Maia. Augmented projections for ptychographic imaging. <http://arxiv.org/pdf/1209.4924.pdf>, 2013.
- [8] J. Sanz. Mathematical considerations for the problem of Fourier transform phase retrieval from magnitude. *SIAM J. Appl. Math.*, 45:651–664, 1985.
- [9] G. Bianchi, R. Gardner, and M. Kilderen. Phase retrieval for characteristic functions of convex bodies and reconstruction from covariograms. *J. Amer. Math. Soc.*, 24:293–343, 2011.
- [10] E. Candes, Y. Eldar, T. Strohmer and V. Voroninski. Phase retrieval via matrix completion. *SIAM J. Imag. Sci.*, to appear.
- [11] R. Remmert. *Theory of Complex Functions*. Springer-Verlag, 1991.
- [12] K. Kreutz-Delgado. *The Complex Gradient Operator and the $\mathbb{C}\mathbb{R}$ -Calculus*. UCSD, 2003.

- [13] C. Yang, J. Qian, A. Schirotzek, F. Maia and S. Marchesini. Iterative Algorithms for Ptychographic Phase Retrieval. arxiv.org/pdf/1105.5628, 2011
- [14] T. Steihaug. The conjugate gradient method and trust regions in large scale optimization. *SIAM J. Num. Anal.*, 20:626–637, 1983.
- [15] P. Thibault and M. Guizar-Sicairos. Maximum-likelihood refinement for coherent diffractive imaging. *New Journal of Physics*, 14(6):063004, 2012.
- [16] S. Marchesini. A unified evaluation of iterative projection algorithms for phase retrieval. *Rev. Sci. Instrum.*, 78:011301, Jan 2007.
- [17] J. Moré and D. J. Thuente. Line search algorithms with guaranteed sufficient decrease. *ACM Trans. Math. Software*, 20(3):286–307, 1994.
- [18] J. Nocedal and S. J. Wright. *Numerical Optimization*. Springer-Verlag, New York, 1999.
- [19] J. R. Fienup. Phase retrieval algorithms: a comparison. *Appl. Opt.*, 21:2758–2769, 1982.
- [20] R. Luke. Relaxed averaged alternating reflections for diffraction imaging. *Inverse Problems*, 21:37–50, 2005.
- [21] S. Marchesini. Phase-retrieval and saddle-point optimization. *J. Opt. Soc. Am. A*, 24:3289–3296, 2007.
- [22] J. M. Rodenburg. Ptychography and related diffractive imaging methods. *Advances in Imaging and Electron Physics*, 150:87184, 2008.
- [23] C. T. Kelley. *Iterative Methods for Optimization*. SIAM, Philadelphia, 1999.
- [24] O. Bunk, M. Dierolf, S. Kynde, I. Johnson, O. Marti, and F. Pfeiffer. Influence of the overlap parameter on the convergence of the ptychographical iterative engine. *Ultramicroscopy*, 108:481–487, 2008.
- [25] Z. Wen, C. Yang, X. Liu and S. Marchesini. Alternating direction methods for classical and ptychographic phase retrieval. *Inverse Problems*, 28:115010, 2012.
- [26] P. C. Hansen. *Discrete Inverse Problems: Insight and Algorithms*. SIAM, Philadelphia, 2010.

DEPARTMENT OF MATHEMATICS, MICHIGAN STATE UNIVERSITY, EAST LANSING, MI 48824
E-mail address: qian@math.msu.edu

COMPUTATIONAL RESEARCH DIVISION, LAWRENCE BERKELEY NATIONAL LABORATORY, BERKELEY, CA 94720.
E-mail address: cyang@lbl.gov

ADVANCED LIGHT SOURCE, LAWRENCE BERKELEY NATIONAL LABORATORY, BERKELEY, CA 94720.
E-mail address: aschirotzek@lbl.gov

NERSC, LAWRENCE BERKELEY NATIONAL LABORATORY, BERKELEY, CA 94720.
E-mail address: frmaia@lbl.gov

ADVANCED LIGHT SOURCE, LAWRENCE BERKELEY NATIONAL LABORATORY, BERKELEY, CA 94720.
E-mail address: smarchesini@lbl.gov